ACS Energy LETTERS

http://pubs.acs.org/journal/aelccp

Stack Pressure Measurements to Probe the Evolution of the Lithium–Solid-State Electrolyte Interface

Chanhee Lee, Sang Yun Han, John A. Lewis, Pralav P. Shetty, David Yeh, Yuhgene Liu, Emily Klein, Hyun-Wook Lee,* and Matthew T. McDowell*

Cite This: *ACS Energy Lett.* 2021, 6, 3261–3269

Read Online

ACCESS | Metrics & More | Article Recommendations | Supporting Information

ABSTRACT: **Although solid-state batteries with lithium metal could enable higher energy density and better safety characteristics than Li-ion batteries, the complex electro-chemo-mechanical evolution of the Li–solid-state electrolyte interface can diminish performance. Here, we measure the stack pressure in real time to provide new insights into the effects of applied stack pressure and electrolyte processing on the interfacial behavior of two representative solid-state electrolytes, $Li_{10}SnP_2S_{12}$ and Li_6PS_5Cl; these materials exhibit different degradation mechanisms through either interphase formation or Li filament growth. We find that stack pressure evolution sensitively depends on interphase formation and that tracking stack pressure coupled with impedance can distinguish between various reaction phenomena and degradation mechanisms within cells. Furthermore, Li filament growth exhibits distinct stack pressure signatures that depend on electrolyte density. The findings advance our understanding of the interfacial evolution of two important classes of solid-state electrolytes, and they demonstrate the utility of electro-chemo-mechanical measurements to understand solid-state battery behavior.**

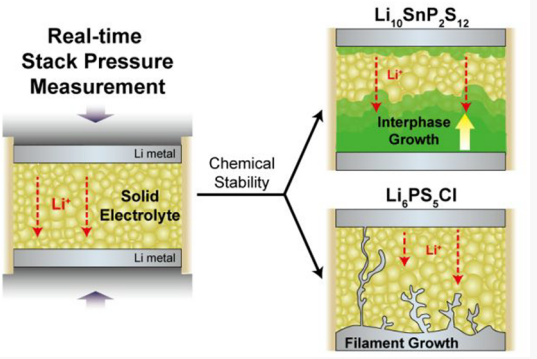

Solid-state batteries (SSBs) are attracting increasing interest largely because of the potential to use lithium (Li) metal as the anode, taking advantage of the high specific capacity and low redox potential of Li.[1,2] The development of SSBs has been accelerated by the discovery of a variety of high-performance solid-state electrolytes (SSEs), including polymers, sulfides, and oxides.[3] Among inorganic SSEs, sulfides are considered promising because of their high ionic conductivity ($>10^{-3}$ S cm^{-1}) and relative ease of processing.[4−7]

Despite these advances, numerous challenges have hindered the use of Li anodes with sulfide SSEs. First, Li metal filaments (also called dendrites or protrusions) can grow during charge to mechanically penetrate the SSE pellet, resulting in short-circuiting and cell failure.[8,9] Defects within the SSE such as pores, grain boundaries, and cracks can affect and/or exacerbate Li filament growth.[10−14] Second, many sulfide SSEs are thermodynamically unstable in contact with Li, resulting in the formation of an "interphase" with different structural, chemical, and transport properties than the pure SSE.[15] The reduction of SSEs at the Li anode tends to result in the formation of a mixture of compounds, and the balance between the electronic and ionic conductivity of the mixture determines the trajectory of interphase growth.[16−18] For example, the reduction of $Li_{10}GeP_2S_{12}$ by Li leads to the formation of binary compounds such as Li_2S, Li_3P, and Li–Ge alloys, and the electronically conducting interphase causes continued interphase growth during electrochemical reduction.[19,20] In contrast, other sulfide-based SSEs form interphases that are electronically insulating and ionically conducting, resulting in limited interphase formation; examples include $70Li_2S$-$30P_2S_5$ ($Li_7P_3S_{11}$) and argyrodite-type Li_6PS_5X (X = Cl, Br, or I).[21−23]

In addition to these challenges, the stack pressure applied to SSBs plays a critical role in determining their performance and must be carefully controlled.[24,25] High stack pressures can induce uniform interfacial contact between Li and the SSE, but they can also mechanically deform and force Li through

Received: July 6, 2021
Accepted: August 18, 2021

https://doi.org/10.1021/acsenergylett.1c01395
ACS Energy Lett. 2021, 6, 3261–3269

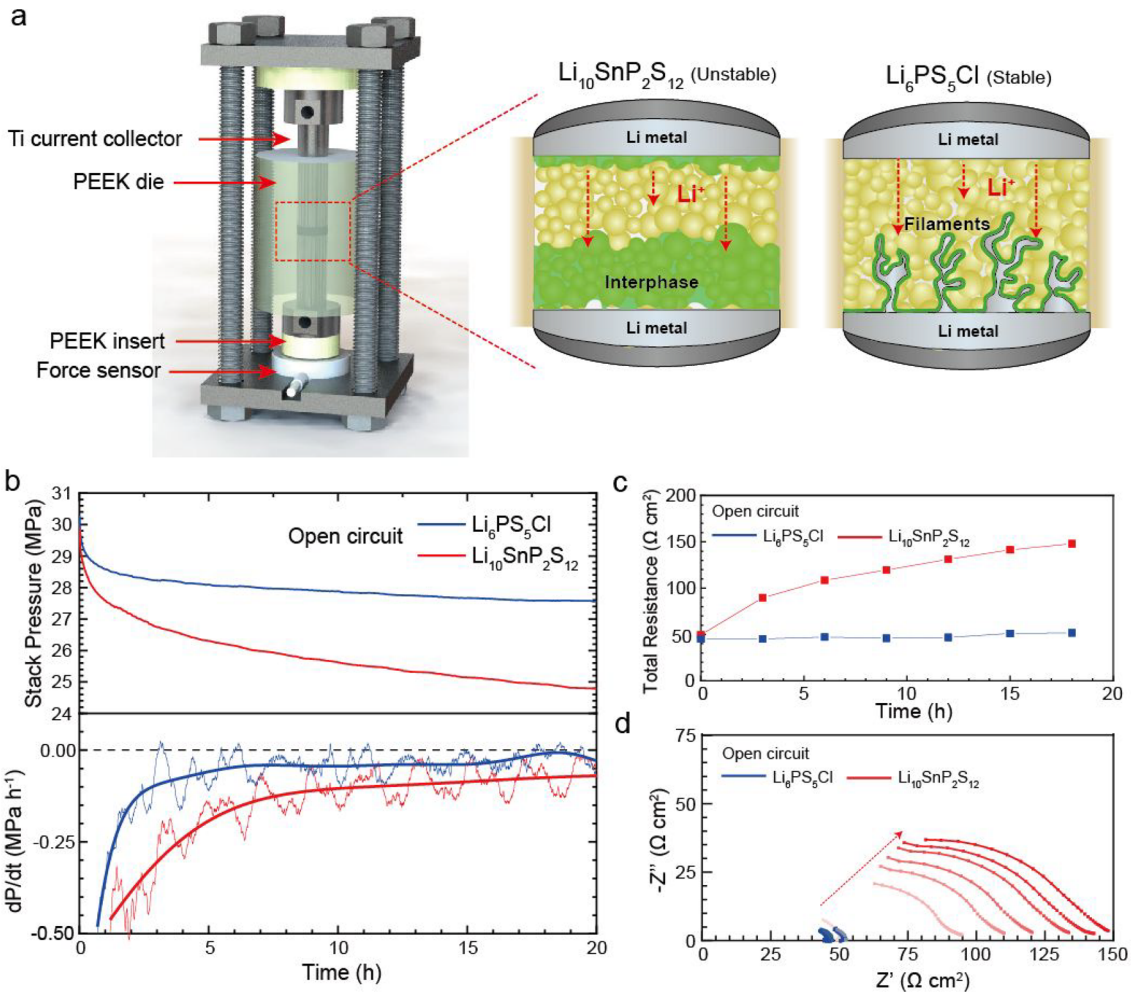

Figure 1. (a) Schematic of the solid-state battery assembly used herein (left) and illustration of the different degradation mechanisms of $Li_{10}SnP_2S_{12}$ (LSPS)- and Li_6PS_5Cl (LPSC)-based symmetric cells (right). (b) Stack pressure evolution after pressing to an initial stack pressure of 30 MPa and holding at open circuit for two different symmetric cells based on LSPS (red) and LPSC (blue). The top panel shows the evolution of stack pressure, and the bottom panel shows the time derivative of the stack pressure (thinner lines), along with thicker trend lines from a polynomial fit. The time derivative of the stack pressure was smoothened with a Savitzky-Golay filter.[33] (c) Plot of total resistance as a function of time for the LSPS (red) and LPSC (blue) cells held at open circuit. (d) Electrochemical impedance spectra measured every 3 h for each cell during the open-circuit hold in (b) used to generate the total resistance plot in (c); total resistance is given as the intersection of the semicircles with the *x*-axis. All pellets used in (b−d) were compacted at 125 MPa during fabrication.

micropores within the SSE pellet to cause short circuits.[8] If the stack pressure is too low, interfacial contact is not sufficient, leading to interfacial void formation during Li stripping.[26] The stack pressure can also vary with cycling due to changes in the volume of active materials, meaning that the actual stack pressure inside the cell can be different than that which is initially applied.[27,28] Interphase formation and morphology evolution at the Li/SSE interface could affect the stack pressure, but such phenomena are not yet well understood. Furthermore, there is a lack of understanding of how the processing parameters and density of the SSE affect dynamic pressure conditions during cycling of SSBs with Li.[29,30] Hence, it is necessary to investigate degradation and failure mechanisms and their correlation with the real-time evolution of stack pressure.

Here, we investigate the interfacial dynamics of Li symmetric cells based on two different representative SSEs ($Li_{10}SnP_2S_{12}$ and Li_6PS_5Cl) by correlating stack pressure measurements to electrochemistry. We find that the evolution of stack pressure is highly dependent on the chemical stability of the SSE in contact with Li, and interphase formation results in a decrease of stack pressure during operation. Li filament growth is shown to exhibit distinct stack pressure signatures that depend on SSE processing and density. These mechanisms are investigated as a function of applied stack pressure and SSE fabrication loads (which control density) to provide comprehensive insight into a variety of degradation regimes for these two important SSE materials. This work provides a new understanding of the interfacial evolution of these materials and demonstrates the value of electro-chemo-mechanical measurements for advancing our understanding of SSBs.

A custom solid-state battery assembly with an integrated force sensor was used for these experiments, as shown schematically in Figure 1a. Symmetric cells with Li electrodes were assembled inside a polyether ether ketone (PEEK) die by first compressing the SSE powders under 62.5, 125, or 250 MPa to form a compacted pellet, and then, Li foil was attached to both sides of the pellet (see the Supporting Information for details). The cell stack was placed on the force sensor and uniaxially pressed to the desired initial stack pressure by

https://doi.org/10.1021/acsenergylett.1c01395
ACS Energy Lett. 2021, 6, 3261−3269

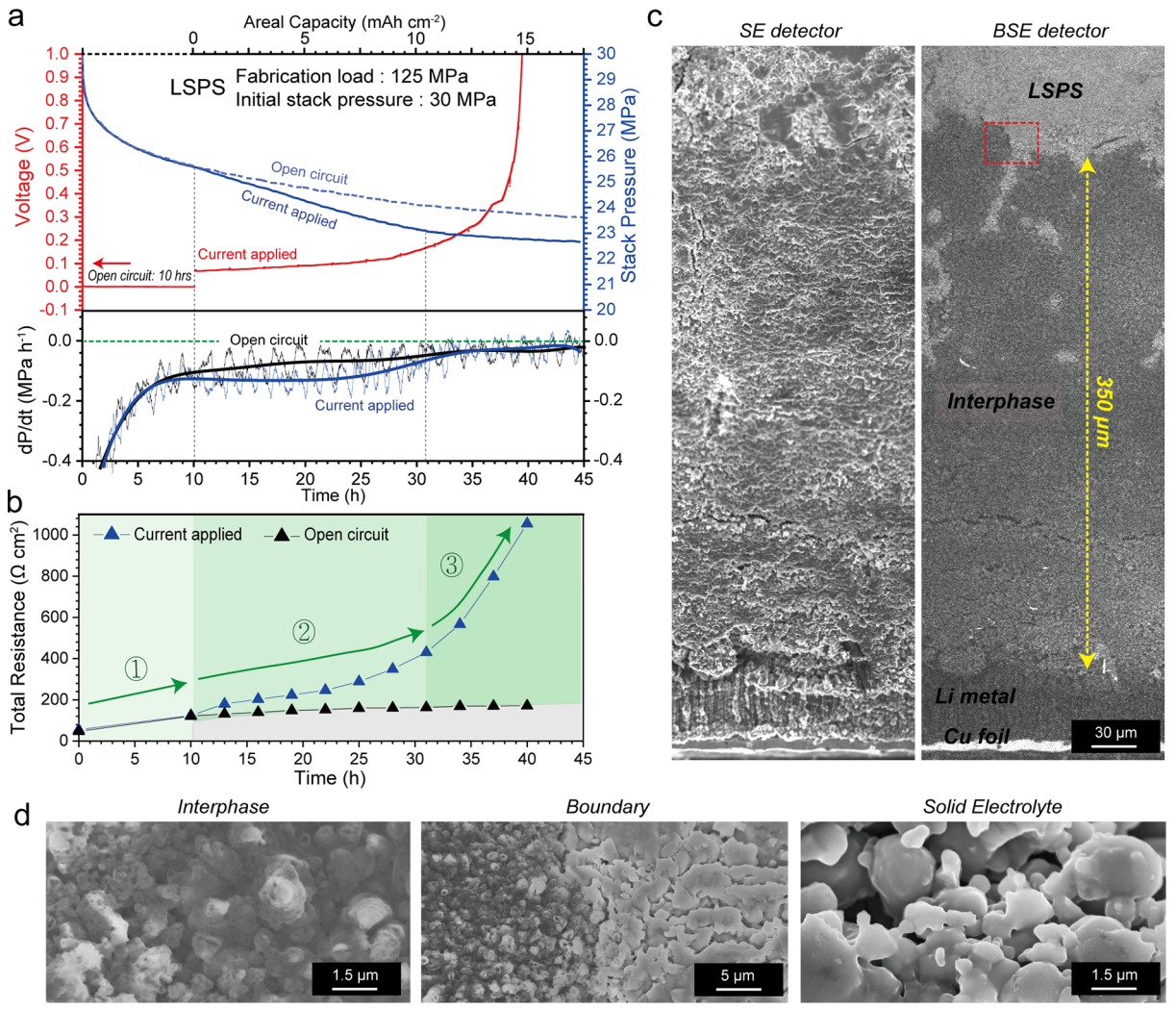

Figure 2. (a) Voltage curves (red) and stack pressure profiles (blue) of two LSPS symmetric cells with initial stack pressure of 30 MPa (top panel) and the time derivatives of the stack pressure with the corresponding trend lines (bottom panel). One cell was operated at 0.5 mA cm^{-2} after being held at open circuit for 10 h (solid lines), and the other cell was held at open circuit for the entire experiment (dotted lines). Both pellets were fabricated by compressing at 125 MPa. (b) Plot of total resistance with time for the cell with current applied (blue) and the cell held at open circuit (black), as extracted from EIS data. (c) Cross-sectional SEM images of the cathodic Li electrode and LSPS from the cell with applied current, using a secondary electron (SE) detector (left) and a backscattered electron (BSE) detector (right). (d) Magnified SEM images of the boundary between the reacted interphase (left) and unreacted LSPS (right) from the cell with the applied current taken from the region with the red box in (c).

tightening the four nuts on top of the cell assembly in Figure 1a, and the stack pressure evolution was then measured with the force sensor during electrochemical cycling. Two different SSE materials were used in this study: $Li_{10}SnP_2S_{12}$ (LSPS) and Li_6PS_5Cl (LPSC). These materials were chosen because of their similar high ionic conductivities (1.9×10^{-3} S cm^{-1} for LSPS and 1.8×10^{-3} S cm^{-1} for LPSC, calculated from electrochemical impedance spectra of Au/SSE/Au cells shown in Figure S1), along with differences in their interfacial stability when in contact with Li metal. Specifically, LSPS is known to form a thick interphase that limits Li filament growth, while LPSC forms a thin and passivating interphase that allows for filament growth (Figure 1a).[16,21]

To understand how stack pressure evolves under open-circuit conditions, Figure 1b shows the stack pressure profiles and the time derivatives of stack pressure (dP/dt, previously termed "differential electrochemical pressiometry")[31] for two different symmetric cells containing LSPS and LPSC with both cells held at open circuit throughout the experiments. The initial stack pressure in both cells was 30 MPa, and the stack pressure of the LSPS cell decreased to 24.8 MPa (red) over the 20 h experiment, while the LPSC cell only decreased to 27.6 MPa (blue). The more substantial stack pressure decrease for the LSPS cell was observed across multiple experiments (Figure S2). The stack pressure decrease at open circuit in these cells is caused by a combination of (1) cell component relaxation, (2) time-dependent deformation of the SSE, (3) plastic deformation and flow of Li metal, and (4) chemical interphase formation. To differentiate among these various contributions, stack pressure evolution was measured in cells with different configurations, including those without Li metal electrodes and without any material components (Figure S3). Without Li metal, the stack pressure change from 30 MPa over 20 h for both SSE materials was less than half that shown in Figure 1b, and it arises from time-dependent deformation of the SSE pellets and relaxation of the cell components. The

https://doi.org/10.1021/acsenergylett.1c01395
ACS Energy Lett. 2021, 6, 3261−3269

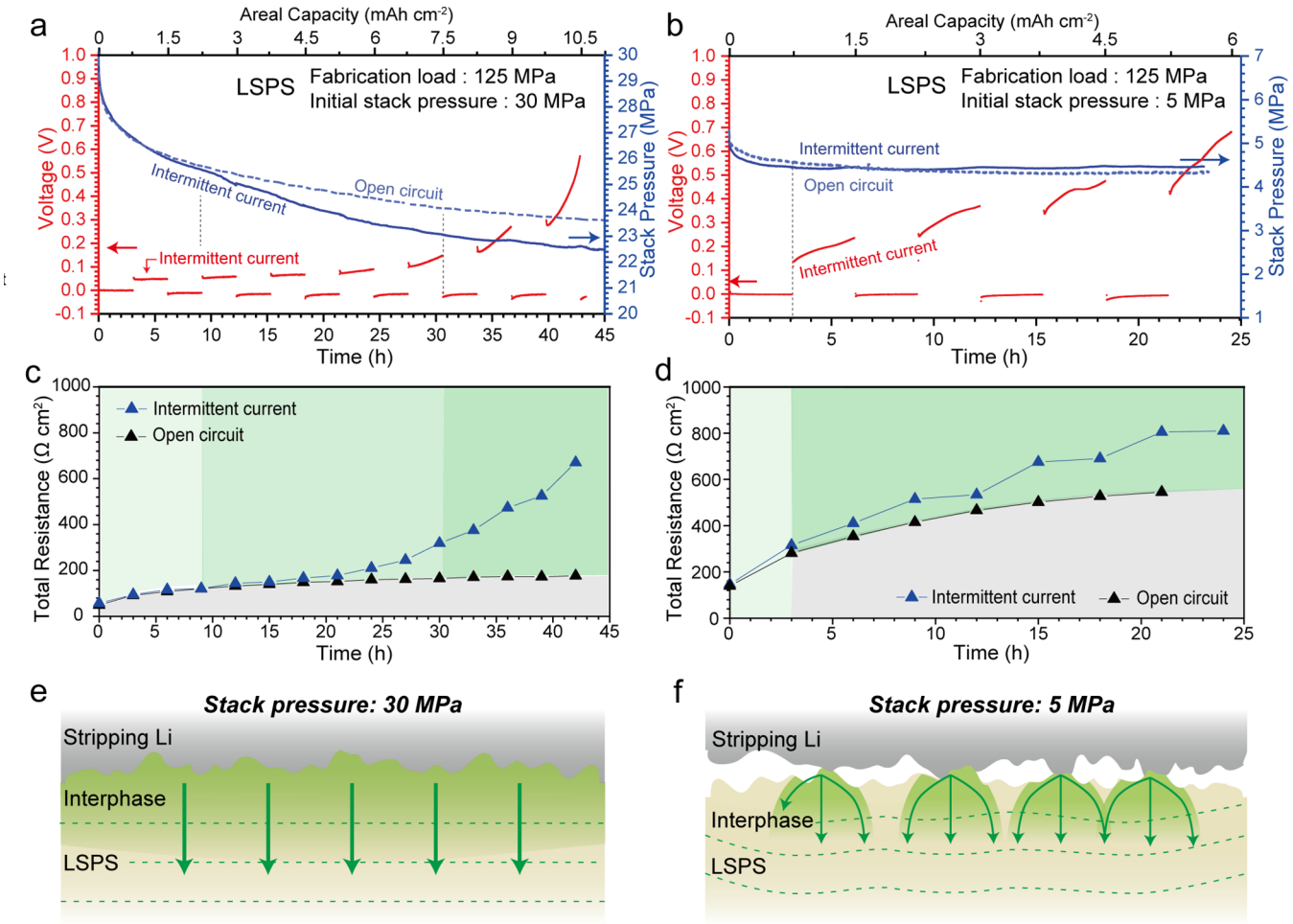

Figure 3. (a) Voltage traces (red) and stack pressure curves (blue) from two LSPS symmetric cells with an initial stack pressure of 30 MPa. Intermittent current was applied to one cell (0.5 mA cm^{-2}, solid lines) with 3 h of current followed by 3 h of open-circuit hold. The second cell was held at open circuit (dotted lines). (b) Voltage traces (red) and stack pressure curves (blue) from two LSPS symmetric cells with a lower initial stack pressure of 5 MPa; one cell had intermittent current applied (0.5 mA cm^{-2}, solid lines), and the other was held at open circuit (dotted lines). (c, d) Evolution of the total resistance extracted from EIS for the two cells with 30 MPa stack pressure (c) and the two cells with 5 MPa stack pressure (d). All LSPS pellets in this figure were fabricated at 125 MPa. (e, f) Schematic illustration of the Li/LSPS interface showing different contact conditions under a higher stack pressure of 30 MPa (e) and a lower stack pressure of 5 MPa (f).

LSPS pellets showed a greater reduction in stack pressure than LPSC under these conditions, which could result from differences in density or time-dependent deformation characteristics of the two SSEs.

The more substantial decreases in stack pressure within the cells that contain Li (Figure 1b) indicate that the deformation of Li and the formation of interphase regions due to the chemical reaction with Li significantly contribute to the stack pressure reduction. The formation of an interphase in a symmetric cell will result in an overall reduction of volume of the cell stack since the molar volume of Li in lithium metal is greater than the partial molar volume of Li in the interphase, and this reduction of volume within the confined cell environment causes the decrease of stack pressure.[20,27] LSPS forms a thicker interphase than LPSC,[16,21,32] which likely contributes to the observed greater decrease in stack pressure for LSPS. Additionally, plastic deformation and flow of Li metal contribute to the greater decrease in stack pressure (Figure 1b) compared to cells without Li (Figure S3), and there could be differences in the extent of Li deformation in contact with the two SSEs.

Further insight into interphase formation is obtained by examining the electrochemical impedance spectroscopy (EIS) data collected every 3 h during these experiments (Figure 1c,d). The total resistance of the LSPS cell increased from 47.9 to 147.6 Ω cm^{-2} after 18 h at open circuit, while the total resistance of the LPSC cell was relatively constant, suggesting that interphase formation in LSPS causes impedance growth. The same trends for both the stack pressure and impedance were observed in other cells with pellets compacted at different loads during fabrication (Figure S2). Since the fabrication load directly affects the density of the pellet, this result indicates that the density of the SSE does not strongly affect interphase formation or Li deformation during the open circuit period. The scanning electron microscopy (SEM) images with a backscattered detector in Figure S4 show an intermediate-contrast interphase region at the interface of LSPS that is ~30−40 μm thick, whereas no discernible interphase region is observed in the LPSC cell.

To investigate the relationship between stack pressure evolution and electrochemistry in LSPS symmetric cells, a current density of 0.5 mA cm^{-2} was applied after holding at open circuit for 10 h. Figure 2a shows the voltage trace from a

https://doi.org/10.1021/acsenergylett.1c01395
ACS Energy Lett. 2021, 6, 3261−3269

symmetric LSPS cell along with the measured stack pressure (solid lines). Figure 2a also shows stack pressure data from a similar LSPS cell with the same amount of Li held at open circuit (dotted line) for comparison. Both cells were pressed to an initial stack pressure of 30 MPa, and the LSPS pellets were fabricated under a load of 125 MPa. During the initial 10 h open-circuit hold, both cells show similar decreases in stack pressure. Upon application of current, however, the stack pressure falls at a faster rate over the next ∼21 h compared to the cell held at the open circuit; these differences in slope are highlighted by the dP/dt curve in the bottom panel of Figure 2a. After ∼31 h of the experiment, the voltage of the applied-current cell rapidly polarizes to 1 V. As this polarization occurs, the slope of the stack pressure curve reduces and again becomes similar in magnitude to the cell held at open circuit (as verified by the similar dP/dt values in the bottom panel of Figure 2a). Figure 2b presents the total resistance measured with EIS from each cell (EIS data are in Figure S5). The impedance of both cells is almost identical after the 10 h open-circuit hold, but the total resistance begins to diverge when current is applied to one cell. The total resistance increases substantially as the voltage of the applied-current cell polarizes to 1 V. Two repeated experiments showed almost identical stack pressure-electrochemistry behavior in multiple cells (Figure S6).

The correlated electrochemistry-stack pressure evolution can be divided into three sections, as shown in Figure 2b. When both cells are at open circuit (section 1), they exhibit the same reduction in the stack pressure and increase in the total resistance. Under applied current, (section 2), the stack pressure drops more rapidly due to electrochemical interphase formation, which contributes to the increased impedance. During this process, voids also likely form at the Li electrode being stripped, which contributes to the impedance increase. It has previously been shown that, in Li/LSPS/Li symmetric cells, Li is stripped at one electrode, while LSPS is electrochemically reduced to form the interphase at the other electrode without substantial Li plating.[20] Cross-sectional SEM images of the cathodic interface from the cell after operation in Figure 2c show that the interphase was ∼350 μm thick, which is much thicker than the cell held at the open circuit in Figure 1b. The magnified SEM images in Figure 2d highlight the differences in the morphology of the interphase vs the pristine LSPS (Figure S5c), and Figure S7 shows EDS results that differentiate between the interphase and pristine LSPS. X-ray diffraction (XRD) was used to investigate structural changes in similar cells after interphase formation (Figure S8), revealing diminished peaks from LSPS and the presence of wide Li_2S peaks. This is consistent with previous studies proving that the interphase contains small Li_2S crystallites.[16,34] The increase in total resistance due to interphase growth thus arises from the presence of phases within the interphase with lower ionic conductivity; for instance, the ionic conductivity of Li_2S ($\sim 10^{-9}$ S cm^{-1}) is much lower than that of LSPS ($\sim 10^{-3}$ S cm^{-1}).[35,36]

In section 3 of the impedance/stack pressure evolution (Figure 2b), the cell polarization increases substantially and the decrease in the stack pressure stabilizes (Figure 2a). This process likely occurs primarily due to contact loss arising from void formation and localized exhaustion of the Li metal due to the large amount of Li passed during the experiment (15 mAh cm^{-2}, approximately 70% of the total Li electrode that was used). Void formation at the stripping electrode has recently been visualized with *operando* X-ray tomography, and loss of interfacial contact is a persistent failure mechanism that is exacerbated by the decrease in stack pressure.[20,24,26] The reduced slope of the stack pressure curve at this point corresponds to a reduction of interphase formation; we emphasize, however, that interphase formation could still contribute to the impedance increase during this period and that voids can form throughout the entire experiment.

We further studied the effects of different initial magnitudes of stack pressure on the evolution of stack pressure/electrochemistry in LSPS symmetric cells (Figure 3). In these experiments, a current density of 0.5 mA cm^{-2} was intermittently applied for 3 h with 3 h open-circuit holds between current periods. Figure 3a,c shows the voltage curves, stack pressure evolution, and total resistances of two cells with 30 MPa applied stack pressure; one had current applied intermittently, and the other was held at open circuit. The results in Figure 3a,c show a similar behavior to Figure 2, where there is a more substantial reduction of stack pressure due to electrochemical interphase formation, followed by eventual loss of contact that drives polarization. During the intermittent current application, dP/dt analysis shows that the slope of the stack pressure curve has a slightly greater absolute magnitude (Figure S9a), and the total resistance of the cell increases to a greater degree after the current application compared to the rest periods (Figure S9b). This is further evidence that the electrochemical reduction promotes interphase growth (Figure S9c), which acts to accelerate stack pressure reduction and the total resistance increase.

In contrast to this behavior, the LSPS symmetric cell with lower initial stack pressure (5 MPa) shows immediate polarization during intermittent current application without substantial deviation of the stack pressure from an identical cell held at open circuit (Figure 3b,d). The immediate polarization is likely due to the poor contact at the interface as the lower stack pressure cannot deform Li to create sufficient interfacial contact. Poor interfacial contact results in highly localized current and the formation of an interphase at contacting points, which contributes to the cell polarization. Evidence for less substantial Li deformation is found from the initial stack pressure drop of ∼0.6 MPa during the first 3 h open circuit period (Figure 3b), which is much smaller than when 30 MPa stack pressure is applied (Figure 2a). Additional analysis of this cell is shown in Figure S10, and the voltage and current curves are shown in Figure S11. The different interfacial evolution scenarios with high and low stack pressure are schematically illustrated in Figure 3e,f.

We have furthermore found that failure through polarization of LSPS symmetric cells is more dependent on the applied stack pressure than the pellet density. Figure S12 shows similar stack pressure evolution and polarization behavior from an LSPS symmetric cell for a pellet compressed at 62.5 MPa (86.4% relative density; see Table S1) instead of 125 MPa (91.3% relative density; see Table S1) when 30 MPa stack pressure is applied. However, for LSPS pellets fabricated at either 62.5 or 125 MPa but under only 5 MPa stack pressure during operation, polarization begins immediately upon applying current (Figure S13), as also shown in Figure 3b,d. Thus, the contact at the interface is the dominant factor that determines the behavior of these cells, rather than the density of the SSE.

We also investigated the coupling of stack pressure and electrochemistry in LPSC-based cells. LPSC forms a thin

https://doi.org/10.1021/acsenergylett.1c01395
ACS Energy Lett. 2021, 6, 3261−3269

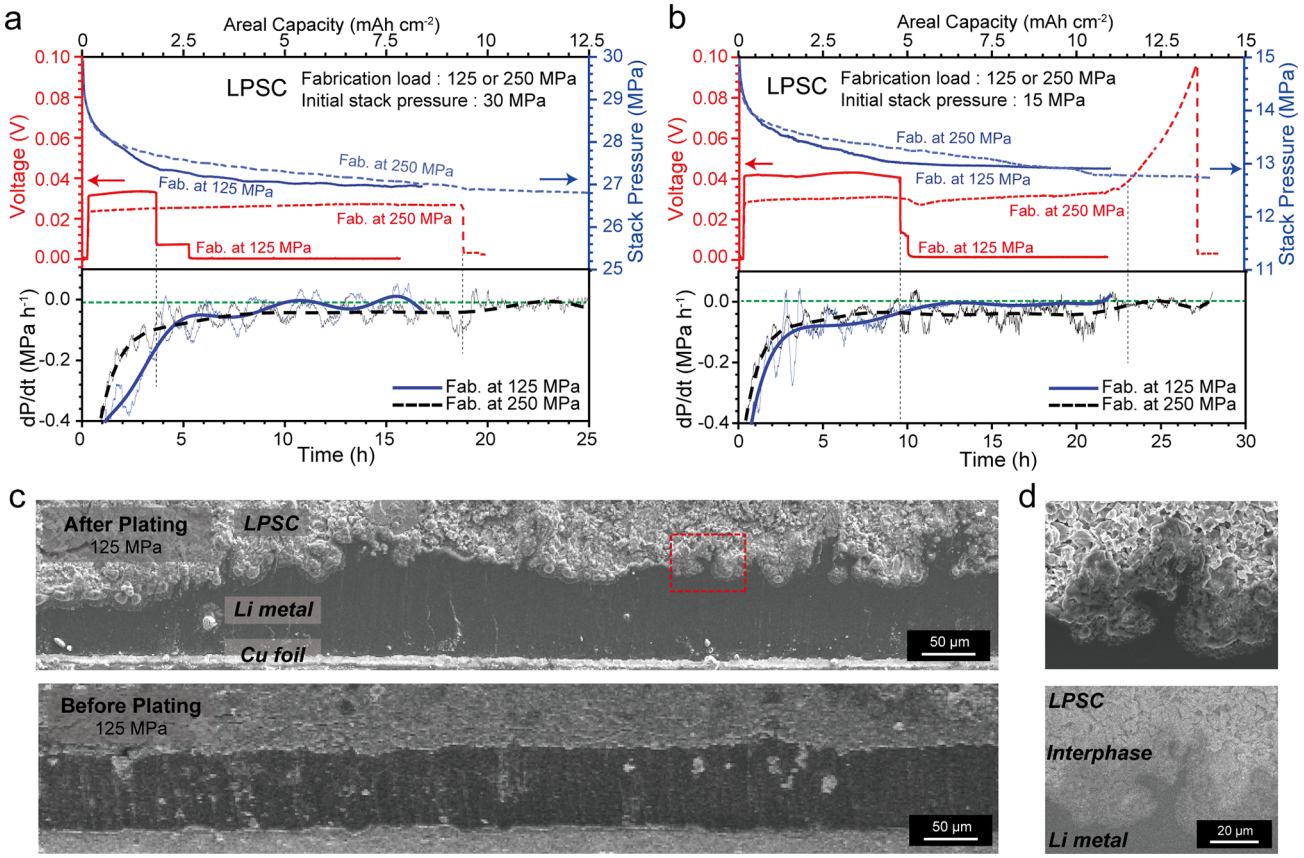

Figure 4. (a, b) Voltage curves (red) and stack pressure evolution (blue) of four LPSC cells with an initial stack pressure of 30 MPa (a) and 15 MPa (b) (top panels), along with the time derivatives of the stack pressure curves (bottom panels). The LPSC pellets were fabricated at either 125 MPa (solid lines) or 250 MPa (dotted lines). All cells were subjected to a current density of 0.5 mA cm^{-2}. (c) Cross-sectional SEM image of a wide region of the cathodic Li electrode from the experiments in panel (b), where 15 MPa stack pressure was applied for a pellet fabricated at 125 MPa (top panel). The bottom panel shows a pristine Li electrode before plating from a sample fabricated at 125 MPa. (d) Magnified SEM images of the red box from (c), including both SE (top panel) and BSE (bottom panel) images.

interphase and is known to allow for Li filaments to grow through the material to cause short circuits, and the interfacial interactions with cathode materials can also cause chemo-mechanical degradation.[8,21,37] However, it is not understood how stack pressure evolves during such processes. We examined LPSC-based symmetric cells with pellets pressed at fabrication pressures of either 125 or 250 MPa under stack pressures of 5, 15, and 30 MPa to understand how these variables affect stack pressure and interface evolution. These fabrication loads of 125 or 250 MPa were chosen because lower values were found to be insufficient to allow for long-duration testing (Figure S14). The distinct behavior of LPSC compared to LSPS fabricated at lower pressures is likely due to different compaction behavior of the powders as well as the different failure mechanisms of these materials. Figure 4a (top panel) shows the voltage and stack pressure profiles of two different cells with LPSC pellets under an initial stack pressure of 30 MPa; the time derivatives of the stack pressure are shown in the bottom panel. A current density of 0.5 mA cm^{-2} was used. The pellet fabricated at 125 MPa (solid lines) supports Li deposition for only 3.67 h (1.84 mAh cm^{-2}) before short-circuiting. In contrast, the more highly compressed pellet (250 MPa, dotted lines) supports Li deposition for 18.8 h (9.41 mAh cm^{-2}) before short-circuiting; such differences in time-to-short-circuit were consistently seen across multiple cells. Thus, under the same initial stack pressure, the fabrication load plays an important role in determining LPSC cell lifetime and short-circuiting behavior.[8,29] In our experiments, the stack pressure was observed to decrease more rapidly for the pellets fabricated at lower pressures, as seen in the pressure trace and the dP/dt curves in Figure 4a. This is likely caused by Li filaments growing to fill pre-existing porosity within the less-dense SSE, which results in a more rapid stack pressure decrease.[14,30,38]

To investigate the density and porosity of the LPSC and LSPS pellets fabricated at different pressures, we carried out density measurements with the Archimedes method (Table S1), and we also visualized the local internal volume of the LPSC pellets with focused-ion beam (FIB) tomography (Figure S15). The LPSC pellets showed 97.8% relative density when fabricated at 250 MPa compared to 92.2% relative density when fabricated at 125 MPa, and the FIB tomographic reconstructions also show a higher density in localized volumes when higher fabrication pressures were used. These measurements support our postulate that Li filaments can grow more easily into pre-existing porosity within the material with lower density (Figure S16).

In addition to the electrochemical growth of Li filaments, the relatively high stack pressure of 30 MPa could also force Li to deform to fill pores within the lower-density pellets, which may contribute to the observed faster short circuits and stack pressure decay. To clarify the effects of electrochemical filament growth versus mechanical deformation of Li on

https://doi.org/10.1021/acsenergylett.1c01395
ACS Energy Lett. 2021, 6, 3261−3269

stack pressure evolution, we performed experiments where two cells fabricated at different loads were first held at open circuit for 10 h and then underwent galvanostatic testing at 0.5 mA cm^{-2} (Figure S17a–c). The decrease in stack pressure was almost identical for the cells during the open circuit period, indicating a similar extent of Li deformation into available pores near the electrodes. Upon the application of current, the stack pressure decreased more substantially for the LPSC pellet with lower density, which again indicates that Li filaments can electrochemically grow to fill pores more easily within the less-dense pellet.

Figure 4b shows similar experiments comparing fabrication loads for LPSC but with a lower initial stack pressure of 15 MPa. Both cells in this figure (with LPSC fabricated at 125 or 250 MPa) sustained longer plating at 0.5 mA cm^{-2} (9.6 h for 125 MPa and 27 h for 250 MPa) compared to the cells at higher stack pressure shown in Figure 4a. This indicates that the stack pressure of 15 MPa is enough to promote good contact at the interface while avoiding the mechanical extrusion of Li into the pores of the pellet upon initial application of stack pressure. Figure 4b also shows that the pellets fabricated at different fabrication loads can exhibit different failure mechanisms. The cell with the pellet fabricated at 125 MPa (solid lines) operates at constant voltage and then short-circuits due to Li filament penetration. After short-circuiting, the stack pressure levels off, as confirmed by the dP/dt curve approaching zero; this indicates termination of electrochemical plating processes in the cell. In contrast, the cell with the pellet fabricated at 250 MPa shows polarization from 0.03 to 0.09 V near the end of the experiment before short-circuiting. This cell polarization is similar to the behavior of the LSPS material in Figures 2 and 3, and it is likely due to void formation and loss of contact at the Li/LPSC stripping interface.[24] The EIS curves for every cell in Figure 4 are presented in Figure S18. Only 54% of the Li metal electrode mass was stripped in this experiment, ruling out the exhaustion of the Li electrode. The stack pressure for this cell became approximately constant during this polarization as contact was lost. These findings were verified through additional experiments on cells that were first held at open circuit for 10 h (Figure S17d–f). Additional related results from LPSC cells with a stack pressure of 15 MPa verified the consistency of these results (Figure S19).

Finally, all cells operated under 5 MPa initial stack pressure exhibited short periods (less than 3 h) of relatively high and rising overpotential before short-circuiting with insignificant changes in stack pressure during these processes (Figure S20). This low stack pressure is not sufficient to establish high-area contact at the Li/LPSC interface, and it leads to isolated contacting points randomly distributed across the interface. The distributed contacting points cause current constriction, which leads to rapid growth and penetration of a few filaments, resulting in short-circuiting regardless of the pellet density.

Figure 4c (top panel) shows a cross-sectional SEM image of the plated Li from the cell in Figure 4b (15 MPa initial stack pressure and 125 MPa fabrication load) with a pristine interface before testing shown in the bottom panel. The Cu current collector, Li, and LPSC are clearly visible in these images. The Li electrode has thickened after plating, and there is possible evidence of nonuniform growth at the Li/LPSC interface, as also shown in the magnified image in Figure 4d. The SEM images in Figure 4d show evidence for interphase formation as regions of intermediate contrast with thicknesses of a few micrometers, which is much thinner than the LSPS case. These regions surround the plated Li metal, implying that interphase formation accompanies Li deposition.

Our electro-chemo-mechanical investigations herein have revealed how the different interfacial behavior of these two solid-state electrolyte materials is related to stack pressure evolution, and we have found that the balance between interphase formation and Li plating is a key aspect of the behavior of these materials. LSPS continuously forms an interphase due to the electronic conductivity of the interphase components.[17,18] Operation of LSPS-based symmetric cells primarily results in interphase formation at the cathodic interface rather than Li plating (Figure 5a), and thus, Li

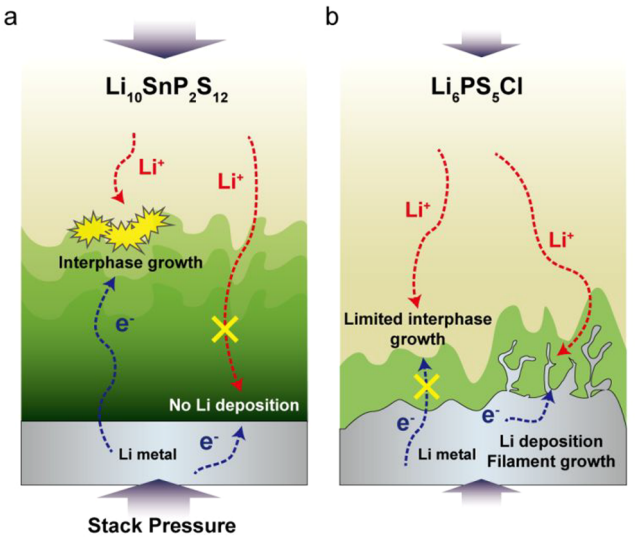

Figure 5. Schematic illustration showing the overall behavior of (a) LSPS and (b) LPSC as determined from our experiments. The vertical arrows denote the relative magnitude of stack pressure reduction during operation of the cell.

filaments do not grow.[20] On the other hand, LPSC forms a thinner interphase that self-passivates due to its electronically insulating characteristics, and potentially nonuniform Li plating occurs simultaneously (Figure 5b).[39] The continual formation of the interphase in LSPS results in a relatively large volume reduction of the cell stack, which translates to an exacerbated reduction of stack pressure in the cell, which is also affected by Li deformation and other processes.[27] In contrast, the stack pressure in LPSC-based cells was found to be primarily affected by the nature of Li filament growth and the availability of open micropores for Li to grow into. These distinct effects in the two different materials result in different magnitudes of stack pressure reduction, and dynamic tracking of stack pressure is thus a powerful diagnostic tool that can provide insight into these phenomena. Future investigation of combined stack pressure/electrochemical evolution with different SSE materials, electrode materials/structures, and full cells is a promising route to establish an improved understanding of the behavior of SSBs, including instabilities at the interfaces. Additionally, such *in situ* stack pressure measurements may be useful as a diagnostic tool for early detection of degradation or faults within operating battery cells.

As we have described in the discussion of our results, the extent of the stack pressure decrease during open-circuit holds

https://doi.org/10.1021/acsenergylett.1c01395
ACS Energy Lett. 2021, 6, 3261–3269

and during current application can be affected by a variety of factors, including Li deformation, SSE porosity, interphase formation, and time-dependent deformation of other cell components. We have performed experiments herein to demonstrate the effects of applied current on the stack pressure trajectory when using two different SSE materials in symmetric cells, which provides insight into the likely mechanisms involved that link electrochemistry and stack pressure. For further understanding and to clearly differentiate some of these mechanistic phenomena, it would be useful in future work to directly relate measured stack pressure evolution to internal cell component evolution via additional characterization experiments, such as X-ray tomography.

■ ASSOCIATED CONTENT

Supporting Information

The Supporting Information is available free of charge at https://pubs.acs.org/doi/10.1021/acsenergylett.1c01395.

Full experimental section, electrochemical impedance spectra, stack pressure evolution and time derivative of the stack pressure, SEM images, voltage and stack pressure profiles, EDS mapping images, XRD patterns, EIS data, voltage and current curves, schematics of LPSC cells, plot of total resistance versus time, and measured density of LSPS and LPSC pellets (PDF)

■ AUTHOR INFORMATION

Corresponding Authors

Matthew T. McDowell − *George W. Woodruff School of Mechanical Engineering and School of Materials Science and Engineering, Georgia Institute of Technology, Atlanta, Georgia 30332, United States;* orcid.org/0000-0001-5552-3456; Email: mattmcdowell@gatech.edu

Hyun-Wook Lee − *Department of Energy Engineering, School of Energy and Chemical Engineering, Ulsan National Institute of Science & Technology (UNIST), Ulsan 44919, Republic of Korea;* orcid.org/0000-0001-9074-1619; Email: hyunwooklee@unist.ac.kr

Authors

Chanhee Lee − *George W. Woodruff School of Mechanical Engineering, Georgia Institute of Technology, Atlanta, Georgia 30332, United States; Department of Energy Engineering, School of Energy and Chemical Engineering, Ulsan National Institute of Science & Technology (UNIST), Ulsan 44919, Republic of Korea*

Sang Yun Han − *George W. Woodruff School of Mechanical Engineering, Georgia Institute of Technology, Atlanta, Georgia 30332, United States*

John A. Lewis − *School of Materials Science and Engineering, Georgia Institute of Technology, Atlanta, Georgia 30332, United States*

Pralav P. Shetty − *George W. Woodruff School of Mechanical Engineering, Georgia Institute of Technology, Atlanta, Georgia 30332, United States;* orcid.org/0000-0002-0583-5707

David Yeh − *School of Materials Science and Engineering, Georgia Institute of Technology, Atlanta, Georgia 30332, United States*

Yuhgene Liu − *School of Materials Science and Engineering, Georgia Institute of Technology, Atlanta, Georgia 30332, United States*

Emily Klein − *School of Materials Science and Engineering, Georgia Institute of Technology, Atlanta, Georgia 30332, United States*

Complete contact information is available at: https://pubs.acs.org/10.1021/acsenergylett.1c01395

Notes

The authors declare no competing financial interest.

■ ACKNOWLEDGMENTS

This work is supported by the National Science Foundation under Award No. DMR-1652471. M.T.M. acknowledges support from a Sloan Research Fellowship in Chemistry from the Alfred P. Sloan Foundation. J.A.L. acknowledges support from a NASA Space Technology Research Fellowship. C.L. and H.-W.L. acknowledge support from the Ministry of Trade, Industry & Energy/Korea Institute of Energy Technology Evaluation and Planning (MOTIE/KETEP) (20194010000100). This work was performed in part at the Georgia Tech Institute for Electronics and Nanotechnology, a member of the National Nanotechnology Coordinated Infrastructure (NNCI), which is supported by the National Science Foundation (ECCS-2025462).

■ REFERENCES

(1) Janek, J.; Zeier, W. G. A Solid Future for Battery Development. *Nat. Energy* **2016**, *1*, 1−4.

(2) Cheng, X. B.; Zhang, R.; Zhao, C. Z.; Zhang, Q. Toward Safe Lithium Metal Anode in Rechargeable Batteries: A Review. *Chem. Rev.* **2017**, *117*, 10403−10473.

(3) Manthiram, A.; Yu, X.; Wang, S. Lithium Battery Chemistries Enabled by Solid-State Electrolytes. *Nat. Rev. Mater.* **2017**, *2*, 1−16.

(4) Chen, S.; Xie, D.; Liu, G.; Mwizerwa, J. P.; Zhang, Q.; Zhao, Y.; Xu, X.; Yao, X. Sulfide Solid Electrolytes for All-Solid-State Lithium Batteries: Structure, Conductivity, Stability and Application. *Energy Storage Mater.* **2018**, *14* (2017), 58−74.

(5) Sakuda, A.; Hayashi, A.; Tatsumisago, M. Sulfide Solid Electrolyte with Favorable Mechanical Property for All-Solid-State Lithium Battery. *Sci. Rep.* **2013**, *3*, 2−6.

(6) Hou, W.; Guo, X.; Shen, X.; Amine, K.; Yu, H.; Lu, J. Solid Electrolytes and Interfaces in All-Solid-State Sodium Batteries: Progress and Perspective. *Nano Energy* **2018**, *52*, 279−291.

(7) Nagao, M.; Hayashi, A.; Tatsumisago, M.; Kanetsuku, T.; Tsuda, T.; Kuwabata, S. In Situ SEM Study of a Lithium Deposition and Dissolution Mechanism in a Bulk-Type Solid-State Cell with a Li_2S-P_2S_5 Solid Electrolyte. *Phys. Chem. Chem. Phys.* **2013**, *15*, 18600−18606.

(8) Doux, J.-M.; Nguyen, H.; Tan, D. H. S.; Banerjee, A.; Wang, X.; Wu, E. A.; Jo, C.; Yang, H.; Meng, Y. S. Stack Pressure Considerations for Room Temperature All-Solid-State Lithium Metal Batteries. *Adv. Energy Mater.* **2020**, *10*, 1903253.

(9) Cao, D.; Sun, X.; Li, Q.; Natan, A.; Xiang, P.; Zhu, H. Lithium Dendrite in All-Solid-State Batteries: Growth Mechanisms, Suppression Strategies, and Characterizations. *Matter* **2020**, *3*, 57−94.

(10) Kazyak, E.; Garcia-Mendez, R.; LePage, W. S.; Sharafi, A.; Davis, A. L.; Sanchez, A. J.; Chen, K. H.; Haslam, C.; Sakamoto, J.; Dasgupta, N. P. Li Penetration in Ceramic Solid Electrolytes: Operando Microscopy Analysis of Morphology, Propagation, and Reversibility. *Matter* **2020**, *2*, 1025−1048.

(11) Liu, H.; Cheng, X. B.; Huang, J. Q.; Yuan, H.; Lu, Y.; Yan, C.; Zhu, G. L.; Xu, R.; Zhao, C. Z.; Hou, L. P.; He, C.; Kaskel, S.; Zhang, Q. Controlling Dendrite Growth in Solid-State Electrolytes. *ACS Energy Lett.* **2020**, *5*, 833−843.

(12) Cheng, E. J.; Sharafi, A.; Sakamoto, J. Intergranular Li Metal Propagation through Polycrystalline $Li_{6.25}Al_{0.25}La_3Zr_2O_{12}$ Ceramic Electrolyte. *Electrochim. Acta* **2017**, *223*, 85−91.

(13) Tian, H. K.; Xu, B.; Qi, Y. Computational Study of Lithium Nucleation Tendency in $Li_7La_3Zr_2O_{12}$ (LLZO) and Rational Design of Interlayer Materials to Prevent Lithium Dendrites. *J. Power Sources* **2018**, *392*, 79−86.
(14) Ning, Z.; Jolly, D. S.; Li, G.; De Meyere, R.; Pu, S. D.; Chen, Y.; Kasemchainan, J.; Ihli, J.; Gong, C.; Liu, B.; Melvin, D. L. R.; Bonnin, A.; Magdysyuk, O.; Adamson, P.; Hartley, G. O.; Monroe, C. W.; Marrow, T. J.; Bruce, P. G. Visualizing Plating-Induced Cracking in Lithium-Anode Solid-Electrolyte Cells. *Nat. Mater.* **2021**, *20*, 1121−1129.
(15) Sang, L.; Haasch, R. T.; Gewirth, A. A.; Nuzzo, R. G. Evolution at the Solid Electrolyte/Gold Electrode Interface during Lithium Deposition and Stripping. *Chem. Mater.* **2017**, *29*, 3029−3037.
(16) Wenzel, S.; Randau, S.; Leichtweiß, T.; Weber, D. A.; Sann, J.; Zeier, W. G.; Janek, J. Direct Observation of the Interfacial Instability of the Fast Ionic Conductor $Li_{10}GeP_2S_{12}$ at the Lithium Metal Anode. *Chem. Mater.* **2016**, *28*, 2400−2407.
(17) Lewis, J. A.; Cortes, F. J. Q.; Boebinger, M. G.; Tippens, J.; Marchese, T. S.; Kondekar, N.; Liu, X.; Chi, M.; McDowell, M. T. Interphase Morphology between a Solid-State Electrolyte and Lithium Controls Cell Failure. *ACS Energy Lett.* **2019**, *4*, 591−599.
(18) Zhu, Y.; He, X.; Mo, Y. Origin of Outstanding Stability in the Lithium Solid Electrolyte Materials: Insights from Thermodynamic Analyses Based on First-Principles Calculations. *ACS Appl. Mater. Interfaces* **2015**, *7*, 23685−23693.
(19) Ong, S. P.; Mo, Y.; Richards, W. D.; Miara, L.; Lee, H. S.; Ceder, G. Phase Stability, Electrochemical Stability and Ionic Conductivity of the $Li_{10\pm1}MP_2X_{12}$ (M = Ge, Si, Sn, Al or P, and X = O, S or Se) Family of Superionic Conductors. *Energy Environ. Sci.* **2013**, *6*, 148−156.
(20) Lewis, J. A.; Cortes, F. J. Q.; Liu, Y.; Miers, J. C.; Verma, A.; Vishnugopi, B. S.; Tippens, J.; Prakash, D.; Marchese, T. S.; Han, S. Y.; Lee, C.; Shetty, P. P.; Lee, H. W.; Shevchenko, P.; De Carlo, F.; Saldana, C.; Mukherjee, P. P.; McDowell, M. T. Linking Void and Interphase Evolution to Electrochemistry in Solid-State Batteries Using Operando X-Ray Tomography. *Nat. Mater.* **2021**, *20*, 503−510.
(21) Wenzel, S.; Sedlmaier, S. J.; Dietrich, C.; Zeier, W. G.; Janek, J. Interfacial Reactivity and Interphase Growth of Argyrodite Solid Electrolytes at Lithium Metal Electrodes. *Solid State Ionics* **2018**, *318*, 102−112.
(22) Wenzel, S.; Weber, D. A.; Leichtweiss, T.; Busche, M. R.; Sann, J.; Janek, J. Interphase Formation and Degradation of Charge Transfer Kinetics between a Lithium Metal Anode and Highly Crystalline $Li_7P_3S_{11}$ Solid Electrolyte. *Solid State Ionics* **2016**, *286*, 24−33.
(23) Zhou, L.; Park, K. H.; Sun, X.; Lalère, F.; Adermann, T.; Hartmann, P.; Nazar, L. F. Solvent-Engineered Design of Argyrodite Li_6PS_5X (X = Cl, Br, I) Solid Electrolytes with High Ionic Conductivity. *ACS Energy Lett.* **2019**, *4* (1), 265−270.
(24) Kasemchainan, J.; Zekoll, S.; Spencer Jolly, D.; Ning, Z.; Hartley, G. O.; Marrow, J.; Bruce, P. G. Critical Stripping Current Leads to Dendrite Formation on Plating in Lithium Anode Solid Electrolyte Cells. *Nat. Mater.* **2019**, *18*, 1105.
(25) McDowell, M. T.; Quintero Cortes, F. J.; Thenuwara, A. C.; Lewis, J. A. Toward High-Capacity Battery Anode Materials: Chemistry and Mechanics Intertwined. *Chem. Mater.* **2020**, *32* (20), 8755−8771.
(26) Wang, M. J.; Choudhury, R.; Sakamoto, J. Characterizing the Li-Solid-Electrolyte Interface Dynamics as a Function of Stack Pressure and Current Density. *Joule* **2019**, *3*, 2165−2178.
(27) Koerver, R.; Zhang, W.; De Biasi, L.; Schweidler, S.; Kondrakov, A. O.; Kolling, S.; Brezesinski, T.; Hartmann, P.; Zeier, W. G.; Janek, J. Chemo-Mechanical Expansion of Lithium Electrode Materials-on the Route to Mechanically Optimized All-Solid-State Batteries. *Energy Environ. Sci.* **2018**, *11* (8), 2142−2158.
(28) Zhang, W.; Schröder, D.; Arlt, T.; Manke, I.; Koerver, R.; Pinedo, R.; Weber, D. A.; Sann, J.; Zeier, W. G.; Janek, J. (Electro)Chemical Expansion during Cycling: Monitoring the Pressure Changes in Operating Solid-State Lithium Batteries. *J. Mater. Chem. A* **2017**, *5*, 9929−9936.
(29) Doux, J. M.; Yang, Y.; Tan, D. H. S.; Nguyen, H.; Wu, E. A.; Wang, X.; Banerjee, A.; Meng, Y. S. Pressure Effects on Sulfide Electrolytes for All Solid-State Batteries. *J. Mater. Chem. A* **2020**, *8*, 5049−5055.
(30) Shen, F.; Dixit, M. B.; Xiao, X.; Hatzell, K. B. Effect of Pore Connectivity on Li Dendrite Propagation within LLZO Electrolytes Observed with Synchrotron X-Ray Tomography. *ACS Energy Lett.* **2018**, *3*, 1056−1061.
(31) Jun, S.; Nam, Y. J.; Kwak, H.; Kim, K. T.; Oh, D. Y.; Jung, Y. S. Operando Differential Electrochemical Pressiometry for Probing Electrochemo-Mechanics in All-Solid-State Batteries. *Adv. Funct. Mater.* **2020**, *30*, 2002535.
(32) Richards, W. D.; Miara, L. J.; Wang, Y.; Kim, J. C.; Ceder, G. Interface Stability in Solid-State Batteries. *Chem. Mater.* **2016**, *28*, 266−273.
(33) Savitzky, A.; Golay, M. J. E. Smoothing and Differentiation. *Anal. Chem.* **1964**, *36* (8), 1627−1639.
(34) Shin, B. R.; Nam, Y. J.; Oh, D. Y.; Kim, D. H.; Kim, J. W.; Jung, Y. S. Comparative Study of TiS_2/Li-In All-Solid-State Lithium Batteries Using Glass-Ceramic Li_3PS_4 and $Li_{10}GeP_2S_{12}$ Solid Electrolytes. *Electrochim. Acta* **2014**, *146*, 395−402.
(35) Huggins, R. A. Recent Results on Lithium Ion Conductors. *Electrochim. Acta* **1977**, *22*, 773−781.
(36) Bron, P.; Johansson, S.; Zick, K.; Der Günne, J. S. A.; Dehnen, S.; Roling, B. $Li_{10}SnP_2S_{12}$: An Affordable Lithium Superionic Conductor. *J. Am. Chem. Soc.* **2013**, *135*, 15694−15697.
(37) Han, Y.; Jung, S. H.; Kwak, H.; Jun, S.; Kwak, H. H.; Lee, J. H.; Hong, S. T.; Jung, Y. S. Single- or Poly-Crystalline Ni-Rich Layered Cathode, Sulfide or Halide Solid Electrolyte: Which Will be the Winners for All-Solid-State Batteries? *Adv. Energy Mater.* **2021**, *11*, 2100126.
(38) Dixit, M. B.; Regala, M.; Shen, F.; Xiao, X.; Hatzell, K. B. Tortuosity Effects in Garnet-Type $Li_7La_3Zr_2O_{12}$ Solid Electrolytes. *ACS Appl. Mater. Interfaces* **2019**, *11*, 2022−2030.
(39) Wang, S.; Xu, H.; Li, W.; Dolocan, A.; Manthiram, A. Interfacial Chemistry in Solid-State Batteries: Formation of Interphase and Its Consequences. *J. Am. Chem. Soc.* **2018**, *140*, 250−257.

https://doi.org/10.1021/acsenergylett.1c01395
ACS Energy Lett. 2021, 6, 3261−3269